IOP Publishing Nanotechnology
Nanotechnology 27 (2016) 095302 (8pp) doi:10.1088/0957-4484/27/9/095302

One-step sol–gel imprint lithography for guided-mode resonance structures

Yin Huang[1], Longju Liu[1], Michael Johnson[2], Andrew C Hillier[2] and Meng Lu[1,3]

[1] Department of Electrical and Computer Engineering, Iowa State University, Ames, IA 50011, USA
[2] Department of Chemical and Biological Engineering, Iowa State University, Ames, IA 50011, USA
[3] Department of Mechanical Engineering, Iowa State University, Ames, IA 50011, USA

E-mail: menglu@iastate.edu

Received 6 November 2015, revised 14 December 2015
Accepted for publication 7 January 2016
Published 29 January 2016

Abstract

Guided-mode resonance (GMR) structures consisting of sub-wavelength periodic gratings are capable of producing narrow-linewidth optical resonances. This paper describes a sol–gel-based imprint lithography method for the fabrication of submicron 1D and 2D GMR structures. This method utilizes a patterned polydimethylsiloxane (PDMS) mold to fabricate the grating coupler and waveguide for a GMR device using a sol–gel thin film in a single step. An organic–inorganic hybrid sol–gel film was selected as the imprint material because of its relatively high refractive index. The optical responses of several sol–gel GMR devices were characterized, and the experimental results were in good agreement with the results of electromagnetic simulations. The influence of processing parameters was investigated in order to determine how finely the spectral response and resonant wavelength of the GMR devices could be tuned. As an example potential application, refractometric sensing experiments were performed using a 1D sol–gel device. The results demonstrated a refractive index sensitivity of 50 nm/refractive index unit. This one-step fabrication process offers a simple, rapid, and low-cost means of fabricating GMR structures. We anticipate that this method can be valuable in the development of various GMR-based devices as it can readily enable the fabrication of complex shapes and allow the doping of optically active materials into sol–gel thin film.

Keywords: nanostructures, sol–gel photonics, imprint lithography, photonic crystal, guided-mode resonant filter

(Some figures may appear in colour only in the online journal)

1. Introduction

Guided-mode resonance (GMR) devices, which are also known as resonant grating waveguides, leaky mode waveguides, or photonic crystal slabs, have the extraordinary capability of generating narrowband reflections at specific wavelengths when illuminated by broadband light. The principle underlying the GMR effect was first established in the early 1990s [1–3]. Subsequently, GMR-based devices have been found to be useful for many applications, including, optical communications, displays, lasers, photovoltaics, and chemical/biological sensing [4–13]. A typical GMR device consists of a substrate, grating coupler, and dielectric waveguide. In addition, the grating coupler can be combined with the waveguide to form a resonant grating waveguide. For a specific combination of incident angle and wavelength, phase matching by the grating allows the incident beam to be coupled into a desired GMR mode [14]. The GMR mode exists because part of the excitation is coupled into the waveguide at resonance, while the rest is either reflected or transmitted. When the light coupled into the grating waveguide leaks outwards, constructive interference between the out-coupled and reflected light yields a sharp resonant reflection peak with nearly 100% efficiency. In contrast, the transmission shows a sharp resonant dip with near 0% efficiency due to the destructive interference between the out-coupled and transmitted light.

The characteristics of a GMR device, such as its resonance wavelength, peak reflection efficiency, and linewidth, are determined by the geometrical parameters of the device

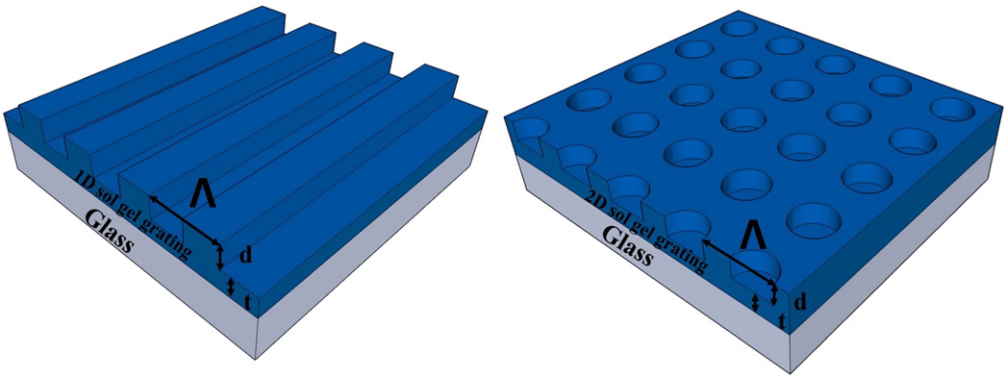

Figure 1. Schematic diagrams of the 1D and 2D sol–gel GMR devices. (a) 1D GMR structure showing the grating patterned on a glass substrate. The grating period (Λ) and depth (d) were $\Lambda = 416$ nm and $d = 150$ nm. (b) 2D GMR structure with the period of $\Lambda = 500$ nm at both *x*- and *y*-directions and depth of $d = 150$ nm. The base layer (t) resides between the grating and the glass substrate, and its thickness was determined by the processing parameters.

and the properties of the constituent materials [15, 16]. Using electromagnetic simulation tools, it is possible to design a GMR that will achieve a desired spectral response. Previously, sub-wavelength GMR gratings that operate in the visible and near-IR wavelength ranges have been fabricated by complex and expensive processes, such as electron beam lithography, focused ion-beam lithography, and deep UV lithography [17–19]. Alternative, bench-top approaches, including interference lithography and nanoreplica molding, have recently been exploited to fabricate sub-wavelength GMR gratings with high throughput, high fidelity, and uniformity [20–23]. Post-lithography processes, such as reactive ion etching and thin-film deposition, are still required to fabricate GMR devices. Unfortunately, these processes increase the overall fabrication complexity and cost. To overcome these issues, we sought to fabricate a grating coupler and waveguide by using a simple, single-step bench-scale process in the form of sol–gel imprint lithography.

In sol–gel imprint lithography, a sol–gel material is used as the imprint resist that transfers a pattern from an elastomer stamp to a desired substrate [23–26]. During the sol–gel imprint process, a colloidal solution, i.e., sol, is converted into a networked gel. The advantages of this process include the low-cost of imprinting and the diverse sol–gel material options. Previous work has demonstrated imprint patterning of sol–gel materials to create the cladding layers of photonic crystal slabs, but without precisely controlled thicknesses and refractive indices of the sol–gel films. Considerable recent progress has been made in creating organic–inorganic hybrid sol–gel materials with high refractive indices [27–30]. The ability to perform imprint lithography using high-refractive-index sol–gel materials provides a new method for fabricating inexpensive and large area GMR devices.

In this study, we demonstrate the single-step fabrication of sol–gel GMR devices using imprint lithography on glass substrates. Sol–gel GMR thin films were formed from organic–inorganic hybrid sol–gel materials to take advantage of their high refractive indices. GMR devices with both 1D and 2D gratings were fabricated and their surface morphologies and optical responses were characterized. The GMR structures supported features as small as 160 nm over areas as large as 8 mm × 8 mm, which is only limited by the imprint template dimensions. When used as optical reflection filters, the sol–gel GMR devices exhibited narrowband reflection upon illumination by broadband light. The influence of processing parameters on the spectral response of the GMR filters was studied. By controlling parameters such as the spin-coating speed and post-imprint bake time, we were able to tune the resonant wavelengths of the GMR devices. When utilized as refractive index sensors, the refractive index changes on the surfaces of the GMR devices led to resonance wavelength shifts. This single-step, sol–gel-based approach offers several distinct advantages, including simplicity, low cost, the ability to tune the GMR resonance, and the potential to incorporate optically active dopants inside the GMR waveguide.

2. Experimental details

Figure 1 presents schematic diagrams of the 1D and 2D sol–gel GMR structures. Both the 1D and 2D sol–gel GMR designs consist of periodically patterned sol–gel films on top of glass substrates. In each case, the refractive index of the sol–gel film (n_{sol}) is greater than the refractive indices of the substrate (n_{glass}) and superstrate (n_{sup}), enabling the structure to function as a waveguide. The period (Λ) and depth (d) of the grating and the base layer thickness (t) determine the resonance wavelength and line shape of the GMR. We sought to design GMR devices in the visible and near infrared wavelength ranges by using a numerical simulation and to subsequently fabricate the structures using sol–gel imprint lithography.

2.1. Optical modeling

A commercial software package employing the rigorous coupled wave analysis method (R-Soft DiffractMOD) was used to model the optical responses of the GMR devices based on the design parameters. For the 1D GMR device,

periodic boundary conditions were applied in the x-direction, while the y-direction was invariant. The reflection spectra perpendicular to the device surface were calculated for both transverse electric (TE) and transverse magnetic (TM) modes. Here, TE is the mode with the electric field (E_y) parallel to the grating direction. The electric field components (E_x and E_z) of the TM mode are perpendicular to the grating. The dimensions of the modeled 1D GMR structure, as determined by measurements of the actual device were: $\Lambda = 416$ nm, $d = 150$ nm, and $t = 130$ nm. Refractive index values of $n_{sol} = 1.8$, $n_{glass} = 1.51$, and $n_{sup} = 1.0$ were assumed in the simulation. To simulate the 2D GMR devices, periodic boundary conditions were applied in both the x- and y-directions. Due to inherent symmetry, the optical response of the 2D GMR device is independent of the polarization state of the incident light. Therefore, an un-polarized plane wave was used as the excitation light source in the simulation. The dimensions of the 2D GMR structure were $\Lambda = 500$ nm, $d = 150$ nm, and $t = 130$ nm. Simulation results are shown in figure 4 and are compared with the experimental measurements.

2.2. Preparation of sol–gel solution

The sol–gel technique was used to fabricate the hybrid organic–inorganic titania film. The precursor solution was prepared by mixing tetrabutyl orthotitanate (TNBT, 244112, Sigma-Aldrich) and diethanolamine (DEA, 16957, Sigma-Aldrich) in ethanol (EtOH 99%). TNBT and DEA were used as the precursor and stabilizer, respectively. The solution was mixed on a magnetic stir plate at room temperature for 2 h. Deionized water (H_2O) and EtOH were pipetted into the precursor solution, which was subsequently hydrolyzed at room temperature. The molar ratio of the chemicals in the solution was TBT:ETA:EtOH:H_2O = 1.2:2:32:1.3. The solution was stirred and homogenized for several hours to form an ethanol-based sol. The sol was gradually aged at room temperature for about five days, while the transparent solution became more viscous and yellow. The aging time was controlled to obtain the viscosity desired for the spin-coating process. All of the chemicals used to synthesize the sol–gel solution were purchased from Sigma-Aldrich and used as received.

2.3. Sol–gel imprint process

We exploited poly(dimethylsiloxane) (PDMS)-based imprint lithography to pattern the sol–gel material into 1D and 2D gratings (figure 2). PDMS was chosen as the mold material because it is gas-permeable and thus facilitates outgassing from the sol–gel while curing without compromising pattern integrity. A PDMS mold possessing a negative surface relief of the desired grating profile was produced by replication of a master silicon grating (figures 2(a) and (b)). The 8 mm × 8 mm silicon master gratings were purchased from LightSmyth Technology Inc. The grating period (duty cycle) of the 1D and 2D silicon master gratings are 416 nm (50%) and 500 nm (50%), respectively. These gratings were cleaned and pretreated using an anti-adhesion coating (Repel Silane, GE Healthercare) to facilitate the subsequent separations. The anti-adhesion treatment was performed by soaking the silicon master in the silane solution for 5 min with a subsequent rinse by using ethanol. To fabricate submicrometer features possessing a 1:1 aspect ratio and high fidelity, we used a two-layer structure consisting of PDMS and hard PDMS (*h*-PDMS) [31]. The *h*-PDMS was prepared by mixing poly(7%–8%vinylmethylsiloxane)-(dimethylsiloxane), 1,3,5,7-tetravinyl-1,3,5,7-tetramethylcyclotetrasiloxane, Xylene, and poly (25%–30% methylhydrosiloxane)-(dimethylsiloxane) (Gelest Inc.) with a weight ratio of 68:2:1:20 and was then spinning it directly onto the silicon master gratings. The *h*-PDMS-coated master gratings were baked at 65 °C for 10 min on a hotplate. A thick layer of, PDMS (Sylgard 184, Dow Corning) was then prepared with a 10:1 ratio of the elastomer to the curing agent and poured onto the *h*-PDMS before curing in a 65 °C oven for 24 h. After being fully cured, each PDMS replica was carefully separated from its silicon grating, as shown in figure 2(b). Before an imprint process, the surface of PDMS mold is thoroughly cleaned in an ultrasonic bath and then treated with an O_2 plasma for 30 s to facilitate the spin coating of sol–gel material.

To fabricate the final GMR structures, the premade sol solution was spun onto the plasma-treated PDMS template. The spin speed was adjusted to manipulate the thickness of the coating. After spinning, a glass coverslip was immediately placed on the sol–gel-coated PDMS, such that the sol visibly filled in the space between the PDMS and the coverslip. To eliminate the defects, the glass coverslips were cleaned using the Piranha clean. The heat-curing process was performed using a hotplate at 200 °C for 5 min while a 300 g calibration weight was placed on the PDMS/sol–gel/coverslip stack to generate a pressure around 50 kPa. Once the sol–gel film had solidified, the flexible PDMS mold was removed (figure 2(f)). The resulting structure was a thin replica grating comprised of highly refractive dielectric TiO_2 film on top of the glass coverslip. The sol–gel film was further annealed at 200 °C to improve the film quality. During the imprint process, the base layer thickness (t) was optimized by varying process parameters including the sol viscosity, spin-coating speed, and applied pressure.

2.4. Optical measurements

The optical response of the GMR devices was characterized using a custom built optical apparatus. Samples were mounted on a kinematic stage to control sample orientation with respect to the incident light beam. A broadband tungsten–halogen light source coupled to an optical fiber with a collimator was used to illuminate the samples. The reflected light was collected at normal incidence using a second optical fiber bundled adjacent to the illumination fiber and was analyzed by a visible spectrometer (USB 2000, Ocean Optics). To characterize the 1D GMR, a linear polarizer was placed between the collimator and the sample to collect both TM or TE oriented light. Unpolarized light was used for measurements with the 2D GMR. All reflection spectra are presented

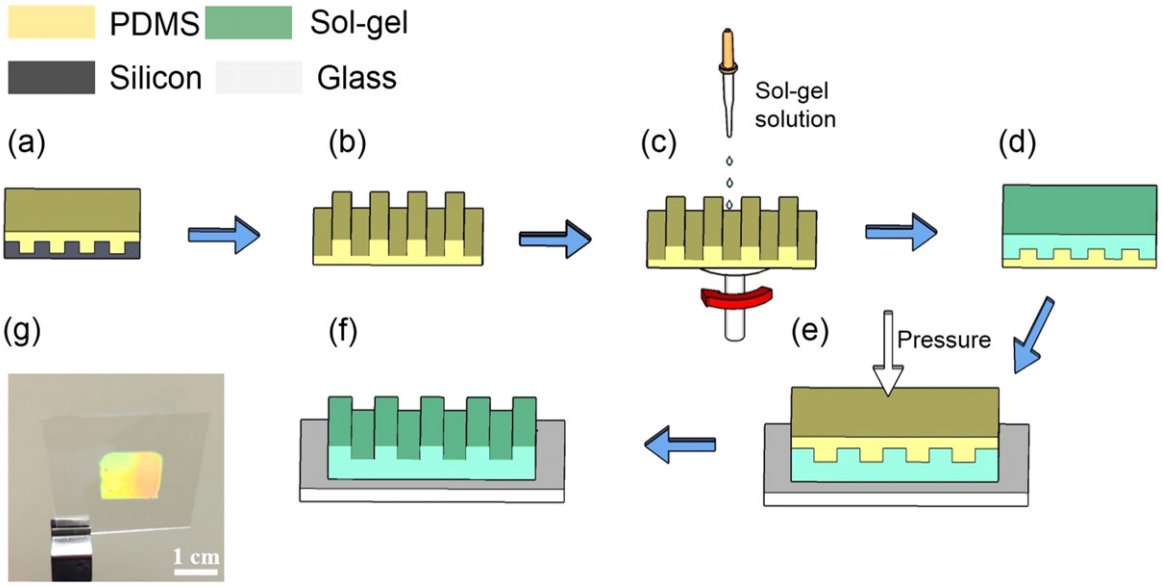

Figure 2. Process flow of the sol–gel imprint process for the fabrication of GMR structures. (a) The PDMS mold is replicated from the silicon master grating. (b) The PDMS mold is separated from the silicon grating and sol–gel solution is spun onto the PDMS mold as shown in (c) and (d). The sol–gel on PDMS is brought into contact with a glass substrate. (e) The PDMS/sol–gel/glass sandwich is baked on a hotplate under a controlled pressure. (f) After solidification of the sol–gel layer, the PDMS mold is removed and the GMR is baked on the hotplate to improve the film quality. A photograph of a 1D GMR is shown in (g).

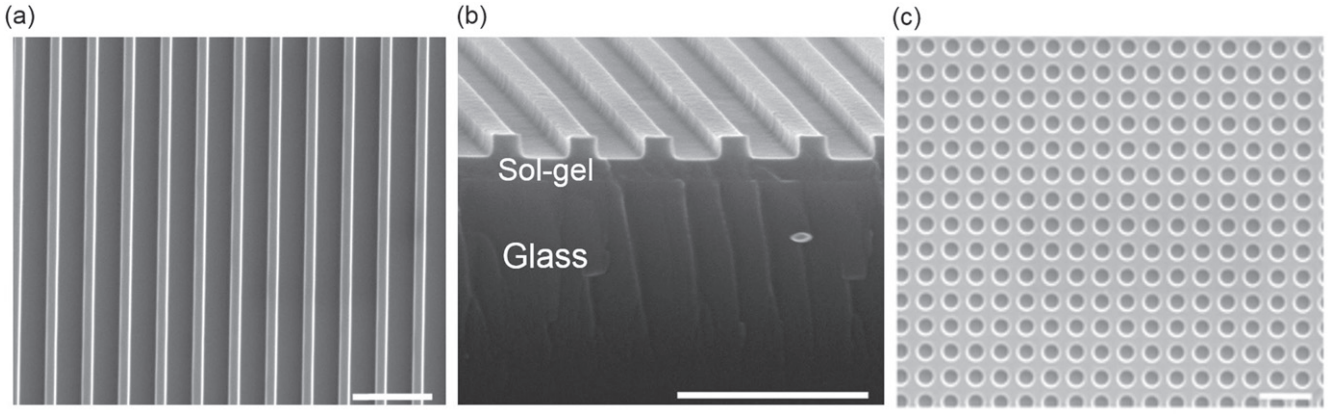

Figure 3. SEM images of sol–gel GMR structures: (a) top view image of the 1D device with $\Lambda = 416$ nm; (b) cross sectional view of the 1D GMR structure showing $d = 150$ nm and $t = 130$ nm; and (c) top view of the 2D GMR structure with $\Lambda = 500$ nm. (Scale bar: 1 μm).

after subtracting the transmission spectra from the incident light.

3. Results and discussion

Several experiments were conducted to characterize the physical and optical properties of the sol–gel GMR devices. Electron microscopy was used to measure structural dimensions and analyze film quality. The optical responses of both 1D and 2D devices were then measured. Using the 1D device as an example, the effects of process parameters on the optical resonance were examined. As a demonstration of application, we performed refractometric sensing measurements using the 1D sol–gel device.

Figure 3 shows scanning electron micrographs (SEMs) of the 1D and 2D sol–gel GMR structures. As depicted in figure 3(a), the 1D pattern consists of periodic ridges with widths of about 160 nm and a pitch of $\Lambda = 416$ nm. A cross-sectional view (figure 3(b)) shows the grating amplitude ($d = 150$ nm) and base layer thickness of approximately130 nm). The 2D grating pattern shown in figure 3(c) is an array of cylindrical holes with diameters of about 300 nm that are arranged in a square lattice with a pitch of $\Lambda = 500$ nm. Within resolution limits, we observed uniform grating structures with minimal defects over the inspected areas. Notably, SEM images suggested that the pitch values of the sol–gel gratings experienced a moderate shrinkage of about 20% over the dimensions of the silicon master gratings following sustained annealing at 200 °C. It is worth noting that there are a few microscopic defects in the

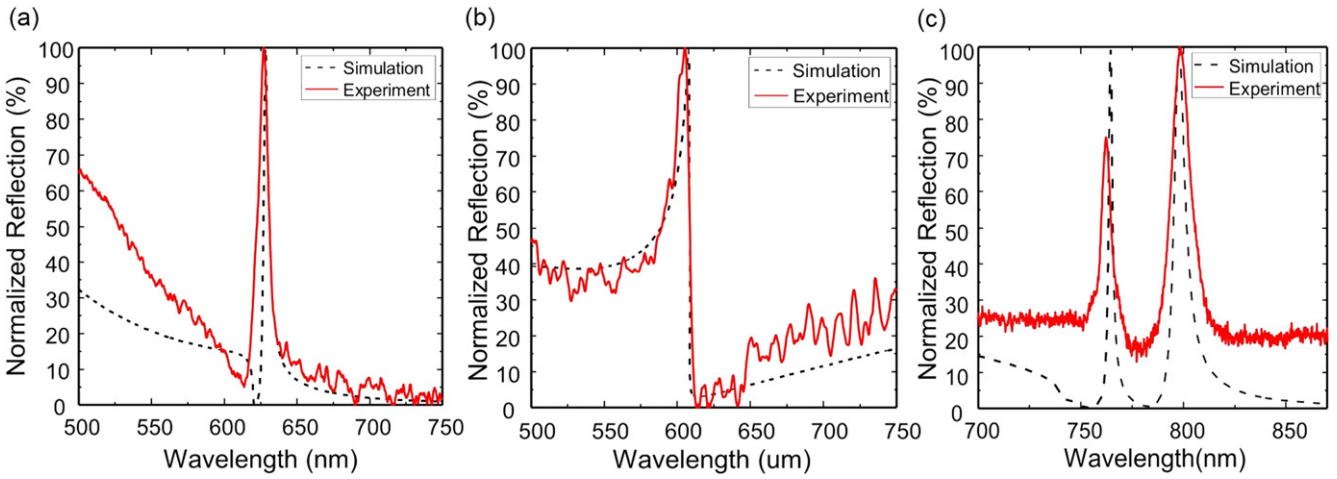

Figure 4. Simulated and experimental reflection spectra at normal for 1D (a) and (b) and 2D (c) GMR structures. The simulated and measured reflection spectra of the 1D GMR structure correspond to dimensions of $\Lambda = 416$ nm, $d = 150$ nm, and $t = 130$ nm with (a) TE and (b) TM polarized light. (c) The simulated and measured reflection spectra of the 2D GMR structure with dimensions of $\Lambda = 500$ nm, $d = 150$ nm, and $t = 130$ nm.

sol–gel grating. The defects only slightly deteriorate the optical response of the GMR on a macroscopic scale.

3.1. Reflection measurements

Figures 4(a) and (b) show the predicted and measured reflection spectra of a 1D sol–gel device at normal incidence under TE and TM illumination, respectively. For this sample, the base layer thickness was $t = 130$ nm. The simulated TE results exhibit a strong resonance centered at $\lambda_{TE} = 629$ nm with a full-width at half-maximum (FWHM) of 4 nm. In comparison, the measured reflection spectrum showed a near exact match of the peak wavelength $\lambda_{TE} = 627$ nm and only a slightly larger width of $FWHM_{TE} = 9$ nm. The TM mode exhibited a peak wavelength of $\lambda_{TM} = 607$ nm with $FWHM_{TM}$ of 20 nm for the simulated results, while the measured wavelength was $\lambda_{TM} = 605$ nm with $FWHM_{TM} = 19$ nm. The small difference between the measured and simulated resonance characteristics are likely the result of using constant refractive index values for the various materials in the simulation. Figure 4(c) compares the simulated and measured reflection spectra of a 2D GMR device. Because the 2D structure was symmetric in the *x*-*y* plane, the incident light was left unpolarized. The simulation results predicted resonance peaks at $\lambda = 764$ nm and 798 nm with TE- and TM mode illumination, respectively, while the corresponding measured spectra exhibited resonance peaks at $\lambda = 762$ nm and 798 nm. These peaks are associated with the TE-and TM modes supported by each direction of the 2D GMR.

3.2. Effect of the base layer thickness

Previous work has demonstrated that the spectral position of the resonant mode depends on the thickness of the waveguide layer, i.e., the sol–gel film thickness. During the sol–gel imprint process, it is possible to control the thickness of the sol–gel base layer by adjusting the rotation speed used during spin coating. For example, decreasing the rotation speed will increase the base layer thickness (t) of this sol–gel film. An increase in the base layer thickness shifts the position of the reflection peak of the GMR mode to longer wavelengths. In order to investigate the effects of the base layer thickness on the resonance characteristics, 1D sol–gel samples were fabricated using different rotation speeds (e.g., 2000, 3000 and 4000 rpm), while the other process parameters remained unchanged. The reflection spectra of these GMR devices were then measured. Figure 5(a) shows the normalized TE reflection spectra for the 1D device with three different base layer thicknesses ($t = 130$ nm, 170 nm, and 200 nm), as determined by cross-sectional SEM images. The resonance wavelengths of the devices with base layer thicknesses of 130, 170 and 200 nm are located at $\lambda_{TE} = 627$ nm, 637 nm, and 647 nm, respectively.

3.3. Tuning of GMR wavelength by post-imprint bake

In addition to the base layer film thickness, the refractive index of the sol–gel film also influences the spectral properties of the corresponding GMR device. The post-imprint annealing on a hotplate at 200 °C can cause the sol–gel refractive index to increase. This change occurs due to the increase in bulk density of the TiO_2 hybrid organic-inorganic gel that occurs during the annealing process. In this study, we exploited the post-imprint annealing process to precisely tune the resonant mode of the 1D GMR device. In order to calibrate the variation in sol–gel refractive index with annealing time, planar thin films were prepared on silicon wafers and annealed for five different time periods (5, 30 min, 2, 4 and 12 h) on a hotplate at 200 °C. The sol–gel thin films were subsequently characterized using ellipsometry (Alpha-SE, J. A. Woollam). The measured refractive indices ranged from 1.726 up to 1.912. The shortest annealing time resulted in a refractive index of 1.73, while the sample that was annealed for 12 h exhibited a refractive index increase up to 1.91. Five

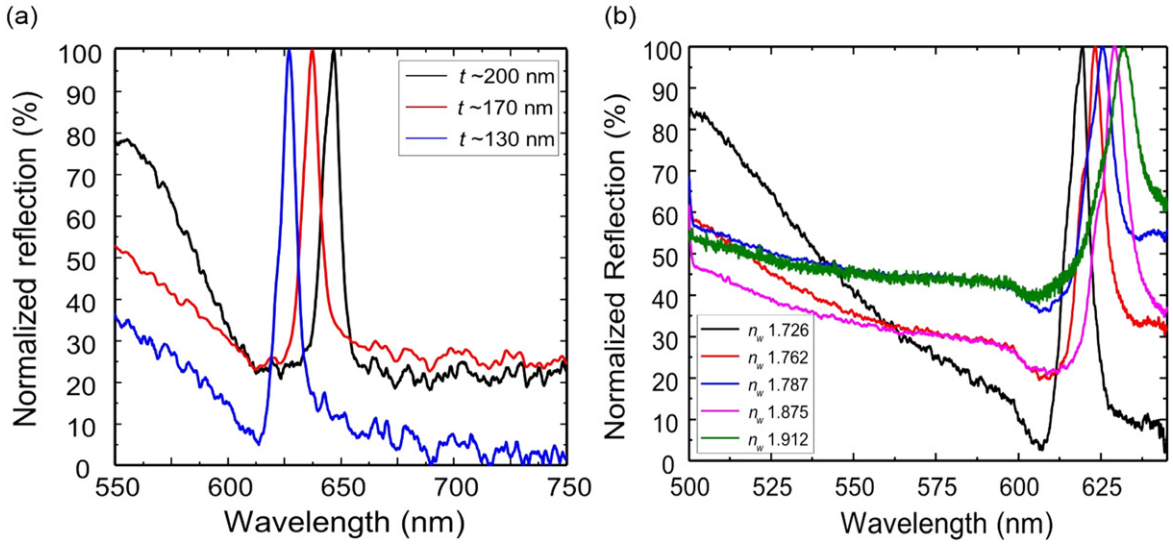

Figure 5. Optical characteristics of the sol–gel GMR devices with different base layer thicknesses and refractive indices. Normalized reflection spectra measured for the 1D sol–gel device with: (a) base layer thicknesses of $t = 130$, 170, and 200 nm; and (b) with sol–gel refractive index values of $n_w = 1.73$, 1.76, 1.79, 1.88, and 1.91. The refractive index values at 632 nm were measured by ellipsometry.

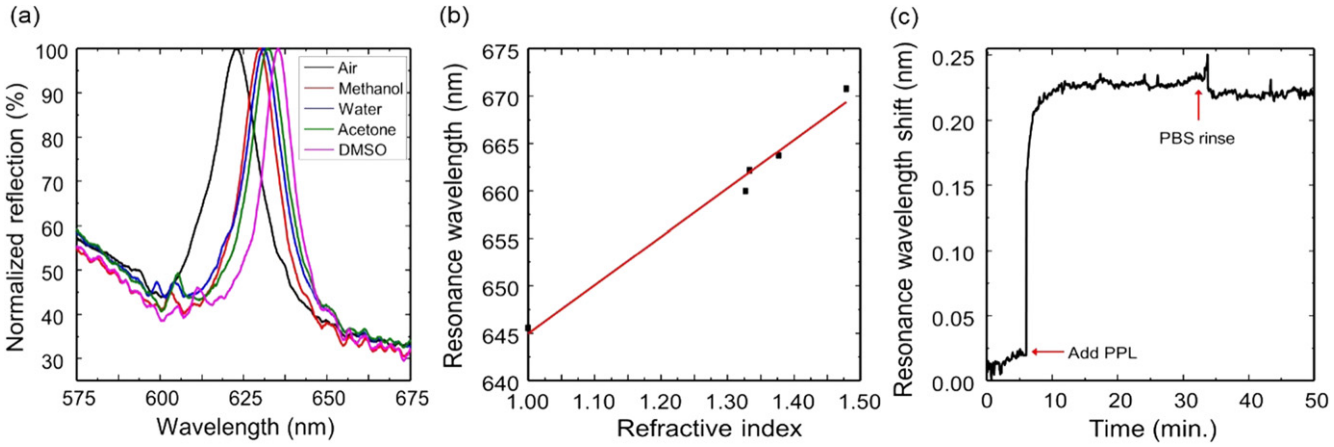

Figure 6. Refractive index based sensing using 1D sol–gel GMR devices. (a) Normalized reflection of the sol–gel GMR sensor when surface was exposed to media with different refractive index values. Five different superstrate materials, air ($n_{sup} = 1.0$), methanol ($n_{sup} = 1.327$), water ($n_{sup} = 1.333$), acetone ($n_{sup} = 1.359$), and DMSO ($n_{sup} = 1.479$) were measured. (b) Refractive index sensitivity of sol–gel GMR sensor characterized by linearly fitting the change in resonant wavelength versus the refractive index value. The sensitivity was calculated to be 50 nm/RIU ($R^2 = 0.99$). (c) Dynamic response of the GMR resonant wavelength when exposed to an aqueous solution containing 0.5 mg ml^{-1} co-poly-l-(lysine, phenylalanine) PPL.

sol–gel GMR samples were imprinted and subsequently annealed for 5 min, 30 min, 2 h, 4 h, and 12 h. Figure 5(b) depicts the normalized reflection spectra measured for each of these samples. As expected, the refractive index increase associated with post-imprint annealing shifted the resonance wavelength from 618 up to 632 nm.

3.4. Application: refractometric sensing

Because the peak wavelength of GMR resonance is sensitive to changes in the optical properties of the surrounding materials, this device can be exploited as a refractive-index sensor. To characterize its sensing performance, we conducted two different tests: (1) resonance measurements in solutions with different refractive index values and (2) detection of the rates of adsorption of a polypeptide film. The reflection spectra of a 1D sol–gel GMR device were measured when the device surface was immersed in five different media: air, methanol, water, acetone, and dimethyl sulfoxide (DMSO), respectively. After each measure, the 1D sol–gel GMR device was dried and used to measure the next solution. The measurement setup is described in section 2.4, where the device is placed horizontally with the surface facing upward. The resonant wavelengths are plotted versus the refractive index of the medium in figure 6(b). A best fit of these results to a straight line give a refractive index sensitivity of $S_b = \Delta\lambda/\Delta n \approx 50$ nm/refractive index unit (RIU).

The sensitivity to surface mass adsorption was characterized by the deposition of a synthetic polypeptide co-poly-l-(lysine, phenylalanine) (poly(Lys, Phe) or PPL, Sigma-

Aldrich), on the sensor surface. When deposited on the device surface, PPL forms a monolayer with a refractive index, thickness, and mass density of 1.45, ~15 nm, and ~2.5 ng mm^{-2} [32], respectively. During the deposition, we recorded the reflection spectra every 10 s, while the resonance wavelength was calculated in real time. The PPL-induced resonance wavelength changes are plotted in figure 6(c). These data were obtained by establishing an initial baseline when the sensor surface was soaked in a phosphate-buffered saline (PBS) solution with pH = 7.4. After 8 min, the PPL solution of 1 mg ml^{-1} was pipetted onto the sample surface and stabilized for 30 min. After about 30 min, the surface was rinsed with PBS solution to remove any weakly bound PPL. After the PPL monolayer had been deposited, the resonant wavelength of the sol–gel device was shifted by approximately 0.25 nm. Compared with the state-of-the-art label-free biosensors [33], the sensitive of the sol–gel GMR device is relatively low. By optimizing the geometry of the grating following the design rules described in [34], we would be able to improve the sensor performances.

4. Conclusion

A single-step, imprint lithography technique was successfully applied to fabricate GMR structures using a high-refractive-index TiO_2-based sol–gel. 1D and 2D grating structures were imprinted in an organic–inorganic hybrid sol–gel film, in which the base layer thickness could be varied and the film's refractive index could be tuned between 1.73 and 1.91. On top of a glass coverslip, this patterned high-refractive-index sol–gel film supported well-defined guided mode resonance. The patterned 1D and 2D gratings showed lattice periods of $\Lambda_{1D} = 416$ nm and $\Lambda_{2D} = 500$ nm, respectively. The processing parameters, including spin speed and post-imprint annealing time, were used to impact the properties and spectral characteristics of the sol–gel GMRs. Fine tuning of the resonant wavelength was achieved by controlling the base layer thickness through the spin coating speed. The film's refractive index could be manipulated via an annealing step. To further demonstrate the utility of these GMR devices, we employed a 1D sol–gel device for refractometric sensing with a sensitivity of 50 nm/RIU. In addition, the sensing device was used to measure the dynamic adsorption of a polypeptide monolayer, exhibiting a resonant wavelength shift of 0.25 nm.

Based on the results of these sol–gel device tests, it is clear that the ability to form GMR structures may prove useful for fabricating inexpensive optical components and biological sensors. With a rapid and simple single-step process and low material cost, sol–gel imprinting represents a viable approach for the fabrication of GMR structures with large surface areas, which are currently only limited by the size of the original master stamp. Because of the ready manipulation of the sol–gel chemistry, we envision this technique can be used to dope these films with optical gain materials [35] in order to explore their applications in the fabrication of active GMR devices, such as surface-emitting distributed feedback lasers.

Acknowledgments

This work was supported by the faculty start-up fund from Iowa State University. ML also acknowledges financial support from 3M through the 3M non-tenured faculty award and support from Northrop Grumman Professorship. ACH acknowledges support from the National Science Foundation through grant CHE 1213582.

References

[1] Day R W, Wang S S and Magnusson R 1996 Filter-response line shapes of resonant waveguide gratings *J. Lightwave Technol.* **14** 1815–24
[2] Wang S S, Magnusson R, Bagby J S and Moharam M G 1990 Guided-mode resonances in planar dielectric-layer diffraction gratings *J. Opt. Soc. Am.* A **7** 1470–4
[3] Rosenblatt D, Sharon A and Friesem A A 1997 Resonant grating waveguide structures *IEEE J. Quant. Electron.* **33** 2038–59
[4] Magnusson R and Shokooh-Saremi M 2007 Widely tunable guided-mode resonance nanoelectromechanical RGB pixels *Opt. Express* **15** 10903–10
[5] Uddin M J, Khaleque T and Magnusson R 2014 Guided-mode resonant polarization-controlled tunable color filters *Opt. Express* **22** 12307–15
[6] Wawro D, Tibuleac S, Magnusson R and Liu H 2000 Optical fiber endface biosensor based on resonances in dielectric waveguide gratings *Proc. SPIE* **3911** 86–94
[7] Huang M C Y, Zhou Y and Chang-Hasnain C J 2007 A surface-emitting laser incorporating a high-index-contrast subwavelength grating *Nat. Photonics* **1** 119–22
[8] Luo S D, Chen L, Bao Y Q, Yang N and Zhu Y M 2013 Non-polarizing guided-mode resonance grating filter for telecommunications *Optik* **124** 5158–60
[9] Mehta A A, Rumpf R C, Roth Z A and Johnson E G 2007 Guided mode resonance filter as a spectrally selective feedback element in a double-cladding optical fiber laser *IEEE Photonic. Technol. Lett.* **19** 2030–2
[10] Polman A and Atwater H A 2012 Photonic design principles for ultrahigh-efficiency photovoltaics *Nat. Mater.* **11** 174–7
[11] Chaudhery V, George S, Lu M, Pokhriyal A and Cunningham B T 2013 Nanostructured surfaces and detection instrumentation for photonic crystal enhanced fluorescence *Sensors* **13** 5561–84
[12] Chen W L, Long K D, Lu M, Chaudhery V, Yu H, Choi J S, Polans J, Zhuo Y, Harley B A C and Cunningham B T 2013 Photonic crystal enhanced microscopy for imaging of live cell adhesion *Analyst* **138** 5886–94
[13] Niraula M, Yoon J W and Magnusson R 2015 Single-layer optical bandpass filter technology *Opt. Lett.* **40** 5062–5
[14] Pokhriyal A, Lu M, Chaudhery V, Huang C S, Schulz S and Cunningham B T 2010 Photonic crystal enhanced fluorescence using a quartz substrate to reduce limits of detection *Opt. Express* **18** 24793–808
[15] Liu J N, Schulmerich M V, Bhargava R and Cunningham B T 2011 Optimally designed narrowband guided-mode resonance reflectance filters for mid-infrared spectroscopy *Opt. Express* **19** 24182–97
[16] Liu J N, Schulmerich M V, Bhargava R and Cunningham B T 2014 Sculpting narrowband Fano resonances inherent in the large-area mid-infrared photonic crystal microresonators for spectroscopic imaging *Opt. Express* **22** 18142–58

[17] Kanamori Y, Kitani T and Hane K 2006 Guided-mode resonant grating filter fabricated on silicon-on-insulator substrate *Japan. J. Appl. Phys.* **45** 1883–5
[18] Bogaerts W, Wiaux V, Taillaert D, Beckx S, Luyssaert B, Bienstman P and Baets R 2002 Fabrication of photonic crystals in silicon-on-insulator using 248 nm deep UV lithography *IEEE J. Sel. Top. Quant. Electron.* **8** 928–34
[19] Balasubramanian K, Heard P J and Cryan M J 2006 Focused ion beam fabrication of two dimensional photonic crystals in silicon-on-insulator *J. Vac. Sci. Technol.* B **24** 2533–7
[20] Rogers J A and Nuzzo R G 2005 Recent progress in soft lithography *Mater. Today* **8** 50–6
[21] Lu M, Choi S, Wagner C J, Eden J G and Cunningham B T 2008 Label free biosensor incorporating a replica-molded, vertically emitting distributed feedback laser *Appl. Phys. Lett.* **92** 261502
[22] Schueller O J A, Whitesides G M, Rogers J A, Meier M and Dodabalapur A 1999 Fabrication of photonic crystal lasers by nanomolding of solgel glasses *Appl. Opt.* **38** 5799–802
[23] Block I D, Chan L L and Cunningham B T 2007 Large-area submicron replica molding of porous low-k dielectric films and application to photonic crystal biosensor fabrication *Microelectron. Eng.* **84** 603–8
[24] Barbé J, Thomson A F, Wang E-C, McIntosh K and Catchpole K 2012 Nanoimprinted TiO_2 sol–gel passivating diffraction gratings for solar cell applications *Prog. Photovolt. Res. Appl.* **20** 143–8
[25] Jeronimo P C, Araujo A N and Conceicao B S M M M 2007 Optical sensors and biosensors based on sol–gel films *Talanta* **72** 13–27
[26] Peroz C, Chauveau V, Barthel E and Søndergård E 2009 Nanoimprint Lithography on silica sol–gels: a simple route to sequential patterning *Adv. Mater.* **21** 555–8
[27] Siddhapara K and Shah D 2012 Characterization of nanocrystalline cobalt doped TiO_2 sol–gel material *J. Cryst. Growth* **352** 224–8
[28] Yoon K M, Yang K Y, Lee H and Kim H S 2009 Formation of TiO_2 nanopattern using reverse imprinting and sol–gel method *J. Vac. Sci. Technol.* B **27** 2810–3
[29] Wang B, Wilkes G L, Hedrick J C, Liptak S C and Mcgrath J E 1991 New high refractive-index organic inorganic hybrid materials from sol–gel processing *Macromolecules* **24** 3449–50
[30] Wang Y B, Flaim T, Mercado R, Fowler S, Holmes D and Planje C 2005 Hybrid high refractive index polymer coatings *Proc. SPIE* **5724** 42–9
[31] Pokhriyal A, Lu M, Chaudhery V, George S and Cunningham B T 2013 Enhanced fluorescence emission using a photonic crystal coupled to an optical cavity *Appl. Phys. Lett.* **102** 221114
[32] Chun G, Lu M, Zhang W and Cunningham B T 2010 Distributed feedback laser biosensor incorporating a titanium dioxide nanorod surface *Appl. Phys. Lett.* **96** 163702
[33] Fan X, White I M, Shopova S I, Zhu H, Suter J D and Sun Y 2008 Sensitive optical biosensors for unlabeled targets: a review *Anal. Chim. Acta* **620** 8–26
[34] Block I D, Ganesh N, Meng L and Cunningham B T 2008 A sensitivity model for predicting photonic crystal biosensor performance *IEEE Sensors J.* **8** 274–80
[35] Stone B T and Bray K L 1996 Fluorescence properties of Er 3 +-doped sol–gel glasses *J. Non-Cryst. Solids* **197** 136–44